Title

Invigoration or Enervation of Convective Clouds by Aerosols?

Journal

Geophysical Research Letters, 48(16)

ISSN

0094-8276

Authors

Igel, Adele L

Heever, Susan C

Publication Date

2021-08-28

DOI

10.1029/2021gl093804

Invigoration or Enervation of Convective Clouds by Aerosols?

Adele L. Igel[1*], Susan C. van den Heever[2]

[1]Department of Land, Air and Water Resources, University of California, Davis; Davis, CA, USA

[2]Department of Atmospheric Science, Colorado State University; Fort Collins, CO, USA

Corresponding author: Adele Igel (aigel@ucdavis.edu)

Key Points:

- Changes to cold-phase processes in polluted storms with cloud base temperature > 290K likely result in weaker, not stronger, updrafts
- Aerosol-induced convective invigoration due to changes in warm-phase processes is theoretically quantified for the first time
- Calculations predict that possible opposing effects in warm- and cold-phases may lead to maximum updraft invigoration well below storm top

This is the author manuscript accepted for publication and has undergone full peer review but has not been through the copyediting, typesetting, pagination and proofreading process, which may lead to differences between this version and the Version of Record. Please cite this article as doi: 10.1029/2021GL093804.

Abstract

Are convective clouds strengthened by the addition of aerosol particles? We present new theoretical calculations which starkly contrast previous results. Prior foundational work suggested that aerosols strongly invigorate convective cloud updrafts via changes to cold-phase processes. We show that the peak magnitude of invigoration by this mechanism is substantially reduced for cold-based storms. For warm-based storms, the updrafts are weakened, not strengthened, by aerosol-induced changes to cold-phase processes. Our calculations show that if invigoration occurs, it is driven primarily by changes to warm-phase processes and may be largest well before the storm reaches maturity. The calculations are based on a new formulation of the moist adiabatic lapse rate that accounts for freezing, supersaturation, and condensate loading. The results significantly reshape our understanding of the impact of aerosols on convective updrafts.

Plain Language Summary

Storms which ingest additional aerosol particles are thought to develop stronger updrafts due to changes in the rates of condensation and freezing of water. We use theoretical calculations to understand the mechanisms that drive this response. Unlike previous studies, we find that aerosol-induced changes to freezing result in weaker storms if the storms have relatively warm cloud bases. Consistent with previous studies, changes to condensation result in stronger storms, but we are the first to theoretically quantify the magnitude of this mechanism. These results suggest that developing storms in polluted environments may often be strongest compared to their clean counterparts well below storm top.

1 Introduction

Tropical and midlatitude convective storms contribute significantly to global precipitation, are crucial for deep vertical mixing of atmospheric constituents, modulate atmospheric radiation, and are projected to change in terms of frequency and intensity with changing climates. The potential for aerosol particles to impact the properties of deep convective clouds has been widely debated. Much of this discussion has fallen under the term "invigoration" though its precise definition is often ambiguous (Andreae et al., 2004; Fan et al., 2013; Hu et al., 2019; Khain et al., 2005; Koren et al., 2014; Koren et al., 2005; Li et al., 2011; Rosenfeld et al., 2008; Stolz et al., 2015; Storer & van den Heever, 2013; Storer et al., 2014; Tao et al., 2012; Thornton et al., 2017; van den Heever et al., 2006). Here we use the term "invigorated" to mean strictly that a storm has the potential for higher updraft speeds.

A number of theories have been postulated about how an increase in the number concentration of aerosols serving as cloud condensation nuclei (CCN) could lead to invigorated storms. These theories concern both the instantaneous invigoration of convection and invigoration through feedbacks on short storm (e.g. Grant & van den Heever, 2015; Lerach et al., 2008; Morrison, 2012; Storer et al., 2010) and longer regional and climate time scales (Abbott & Cronin, 2021; Chua & Ming, 2020; van den Heever et al., 2011). The focus of this study is on the instantaneous invigoration that may occur during the developing phase of the storm.The instantaneous invigoration theories largely fall into two categories: cold-phase and warm-phase.

Cold-phase aerosol invigoration was most prominently hypothesized by Rosenfeld et al. (2008), hereafter R08. They considered a perfectly clean storm as one in which condensate is produced and instantaneously removed from the storm as precipitation. In contrast, a polluted storm is one that lofts the condensed water until it is frozen and removed from the storm. The additional latent heat release upon freezing and the subsequent immediate unloading of the condensate serve to increase the buoyancy above that of the clean storm. The polluted storm is therefore invigorated (has stronger updrafts) relative to the clean storm. Many studies report evidence of increased freezing in deep convective storms to support this hypothesis (Altaratz et al., 2014; Andreae et al., 2004; Fan et al., 2013; Khain et al., 2005; Storer & van den Heever, 2013; van den Heever et al., 2006).

Warm-phase aerosol invigoration refers to the idea that higher aerosol loadings and hence higher cloud droplet concentrations will result in faster condensation rates and a lower supersaturation in the storm core (Fan et al., 2018; Fan et al., 2007; Grabowski & Jarecka, 2015; Grabowski & Morrison, 2016; Kogan & Martin, 1994; Koren et al., 2014; Pinsky et al., 2013; Saleeby et al., 2015; Seiki & Nakajima, 2014; Sheffield et al., 2015). The additional latent heat release from condensation drives the enhanced buoyancy and updraft speeds. The enhanced condensation may come immediately above cloud base (Pinsky et al., 2013) or may not be important until the secondary activation of ultrafine aerosol particles above cloud base (Fan et al., 2018).

Aerosol-induced invigoration, particularly cold-phase aerosol invigoration, has been severely criticized. Some have argued that the magnitudes of invigoration theoretically estimated by R08 are much too large and that aerosol-induced invigoration is not distinguishable from natural co-variability in environmental conditions (Grabowski, 2018; Lebo, 2018). Such an argument is supported by some simulations (Grabowski, 2015; Lebo & Seinfeld, 2011). A recent model intercomparison study demonstrated consistent increases in updraft speeds in response to

increased aerosol loading within the warm-phase but mixed updraft responses in the cold-phase regions (Marinescu et al., 2021). Here we present new theoretical calculations based on first principles to quantify invigoration due to warm- and cold-phase processes. The results starkly contrast with our previous theoretical understanding of this process and provide new insight into the mechanisms and magnitude of aerosol-induced invigoration.

2 Methods

We use convective available potential energy (CAPE) to quantify the potential strength of a storm. Traditional formulations for CAPE neglect ice processes and condensate loading, and assume that supersaturation is removed instantaneously. To relax these assumptions in order to better represent reality, we first derived an expression for the moist adiabatic lapse rate that allows for freezing, condensate loading, and specified supersaturation in order to assess the impacts of these processes on CAPE. We follow the derivation of Früh and Wirth (2007), but rather than using their "mixed phase saturation vapor pressure" we specify the vapor pressure p_1 as the product of the saturation ratio S and the saturation vapor pressure with respect to liquid water p_{21}. The final form of the lapse rate is

$$\frac{dT}{dp} = \frac{\frac{TR_0}{p_0} + \frac{L_{F1} r_1}{p_0}\left(1 - \frac{p}{S}\frac{dS}{dp}\right)}{c_p + L_{32} r_F \frac{d\xi}{dT} + L_{F1} r_1 \frac{p}{p_0}\frac{d \ln p_{21}}{dT}} \tag{1}$$

where T is temperature, p is pressure, R is the gas constant, and r is mixing ratio. Subscript 0 refers to dry air, 1 to the vapor phase, and F to total condensate. $\boldsymbol{\xi}$ is the liquid fraction, $\boldsymbol{L_{21}}$ ($\boldsymbol{L_{32}}$) is the specific heat of vaporization (freezing) and $\boldsymbol{L_{F1}}$ linearly weights the latent heats of vaporization and sublimation according to the liquid fraction. Finally, c_p accounts for the specific heat of the dry air, water vapor, and condensate in the parcel. A full derivation of this equation is given in the supplemental information.

Eq. 1 is numerically integrated to solve for temperature, water vapor, and liquid and ice mixing ratio as a function of pressure assuming a cloud base pressure of 960 hPa and a cloud top pressure of 200 hPa. These quantities are used to calculate density temperature defined as

$$T_\rho = \frac{T\left(1 + \frac{R_1}{R_0} r_1\right)}{1 + r_1 + r_F} \tag{2}$$

(Xu & Emanuel, 1989). The difference in CAPE ($\boldsymbol{\Delta CAPE}$) between two parcels A and B is calculated as

$$\Delta CAPE = \int_{960mb}^{200mb} -R_0 \frac{T_{\rho,A} - T_{\rho,B}}{p}\, dp \tag{3}$$

It is critical to note that the difference in CAPE between two parcels is independent of the environment in which they develop.

Finally, if all CAPE is converted to kinetic energy associated with upward vertical motion, then the difference in CAPE between two parcels is equivalent to $\frac{1}{2}(\boldsymbol{w_A^2 - w_B^2})$. Rearranging this expression yields

$$\Delta w = w_A - w_B = \sqrt{w_B^2 + 2\Delta CAPE} - w_B \quad (4)$$

3 Results

3.1 Cold-phase invigoration

We first review the calculations in R08. R08 assumed that a developing storm in a clean environment instantaneously unloads all condensate and that condensate is formed by deposition at temperatures below -4°C. A polluted developing storm on the other hand retains all condensate until it is frozen and then instantaneously removed. Maximum invigoration occurs when this instantaneous freezing and instantaneous unloading occurs at -4°C. We make these same assumptions except that freezing occurs nearly isothermally between -3 and -4° C rather than isobarically. The use of nearly isothermal freezing rather than isobaric freezing results in about 3 J kg^{-1} per g kg^{-1} of condensate less CAPE due to changes in the timing of the unloading (inferred from Fruh and Wirth 2007) which is minimal. The difference in density temperature (ΔT_ρ) between the polluted and clean storms for this maximum invigoration scenario is shown in Figure 1a (red line). We also add another scenario not considered by R08 (purple line), in which the lofted condensate in the polluted storm is frozen but not unloaded. In both cases, the clean parcel assumptions are identical.

As discussed in R08 and in Grabowski and Morrison (2020), the latent heat released from freezing the liquid condensate approximately balances the condensate loading and therefore brings ΔT_ρ to near zero for both scenarios (point A in Figure 1a). Notably though, point A is at $\Delta T_\rho < 0$. This is true not just for the example shown but for all cases. The gain in ΔT_ρ is less than what is expected from freezing all the liquid ($L_{32} r_F$) because the latent heat released from freezing slows the condensation rate (or even induces evaporation). The actual change in temperature from condensate freezing may be estimated following Emanuel (1994) and is roughly half of the temperature change predicted by $L_{32} r_F$. This reduction in condensation lessens the polluted parcel's gain in buoyancy such that the freezing of condensate in the polluted parcel is insufficient to make it buoyant relative to the clean parcel.

It is the subsequent unloading of condensate following freezing (point B along the red line) that gives rise to the substantial positive ΔT_ρ relative to the ultra-clean scenario and ultimately drives the invigoration. Without the unloading of the frozen condensate (purple line), ΔT_ρ is negative through most of the parcel's ascent. As a result, a polluted storm will be weaker than a clean storm *even though additional freezing of condensate is occurring*. The invigoration described by R08 is typically attributed to the additional freezing of condensate, but the preceding analysis clearly shows that the invigoration is in fact due to the assumption of total unloading of condensate upon freezing in addition to the freezing itself.

As neither unloading of condensate nor freezing is an instantaneous process, we repeat the calculations with more realistic assumptions. We now assume that the fraction of frozen condensate increases linearly between -4 °C and -40 °C. Whereas instantaneous freezing is too rapid, this new assumption likely represents freezing that is too slow (Hu et al., 2010). This is ideal from a theoretical perspective because this assumption gives us something approximating a realistic lower bound on the possible invigoration due to freezing. We also assume that condensate unloading begins when the condensate mixing ratio reaches some threshold. Thereafter the condensate mixing ratio is held constant in the warm-phase and decreases linearly between -4°C and -40°C to some specified unloaded fraction based on the supposition that freezing promotes unloading. A condensate loading threshold of 0 g kg^{-1} corresponds to immediate and complete unloading regardless of the final unloaded fraction and an unloaded fraction of 0 means that the condensate increases until it reaches the condensate loading threshold and remains constant thereafter. When the unloaded fraction is 1, the condensate decreases to 0 at -40°C. See the supplemental information for full details.

Calculations are performed for all combinations of loading thresholds of 0 to 10 g kg^{-1}, unloaded fractions of 0 to 1, and initial parcel temperature (cloud base temperature, T_{CB}) of 280K to 300K to encapsulate a wide range of possible values in reality. For each T_{CB}, the maximum and minimum invigoration value relative to the ultra-clean parcel is found and displayed by the gray lines in Figure 1b. These can be thought of as the lowest possible lower bound and the highest possible lower bound. Figure 1b shows that weak invigoration (up to about 100 J/kg) may occur if T_{CB} is about 292K or less; otherwise, the cold-phase processes lead to weakening, or enervation of the convection. Under the more realistic assumptions, the maximum enervation is reduced (the gray dashed line compared to the unrealistic purple line). The results are somewhat sensitive to the choice of initial and final freezing temperatures. Ending freezing at -20 °C allows for slightly greater invigoration whereas delaying freezing to begin at -15°C and end at -40°C does the opposite. Hereafter we only show results for freezing between -4°C and -40°C.

Figures 1c-d show ΔCAPE as a function of condensate loading threshold and unloaded fraction for cold- and warm-based storms, respectively. While the absolute values shown on the figures are useful for understanding ΔCAPE relative to the ultra-clean parcel, important conclusions can also be drawn from them by examining the gradients of ΔCAPE with respect to the two axes. A positive gradient indicates invigoration and a negative gradient indicates enervation.

Weak invigoration occurs in cold-based storms when the unloading is delayed (i.e. a higher loading threshold). Conversely, storms are slightly weakened if the final unloading is reduced (i.e., lower unloaded fraction) (Fig. 1c). In contrast, in warm-based storms, a polluted parcel is expected to be enervated even when unloading is delayed (Fig. 1d). To understand this difference in response, sample profiles of ΔT_ρ for T_{CB} of 280K and 300 K are shown in Fig. 1a (gray lines). The figure shows that, under our more realistic assumptions, even when enervation occurs, the polluted parcel is still the more buoyant parcel at 200 hPa. The freezing and unloading do make the polluted parcel more buoyant, but the speed at which these processes occur is reduced compared to those under the original assumptions in R08. As a result, in warm-based storms their impacts are not great enough to overcome the low-level weakening from condensate loading, whereas in cold-based storms, the weakening is confined to a shallower layer in the lower part of the storm and weak invigoration is possible.

It is difficult to directly compare these theoretical calculations to previous results from the literature since most studies do not focus on the developing phase of storms and most studies take a Eulerian rather than Lagrangian view of aerosol effects in storms. Nonetheless, the recent model intercomparison study from Marinescu et al. (2021) shows qualitative support for our basic assumptions and results. In that study, five of seven models produced higher condensate loading in the mixed phase region which supports our assumption that higher condensate loading is associated with greater aerosol concentrations. Models were also in disagreement about whether temperatures near the top of the mixed phase layer should be warmer or cooler in polluted storms, which is in agreement with our result that the temperature difference at that level should be small and near zero.

The central panel of Figure 2 schematically represents the key points of these calculations for warm-based storms. Namely, that 1) enervation due to condensate loading dominates through most of the parcel rise and 2) the extra latent heat release from freezing does counteract some of the enervation but is typically not great enough to lead to net invigoration.

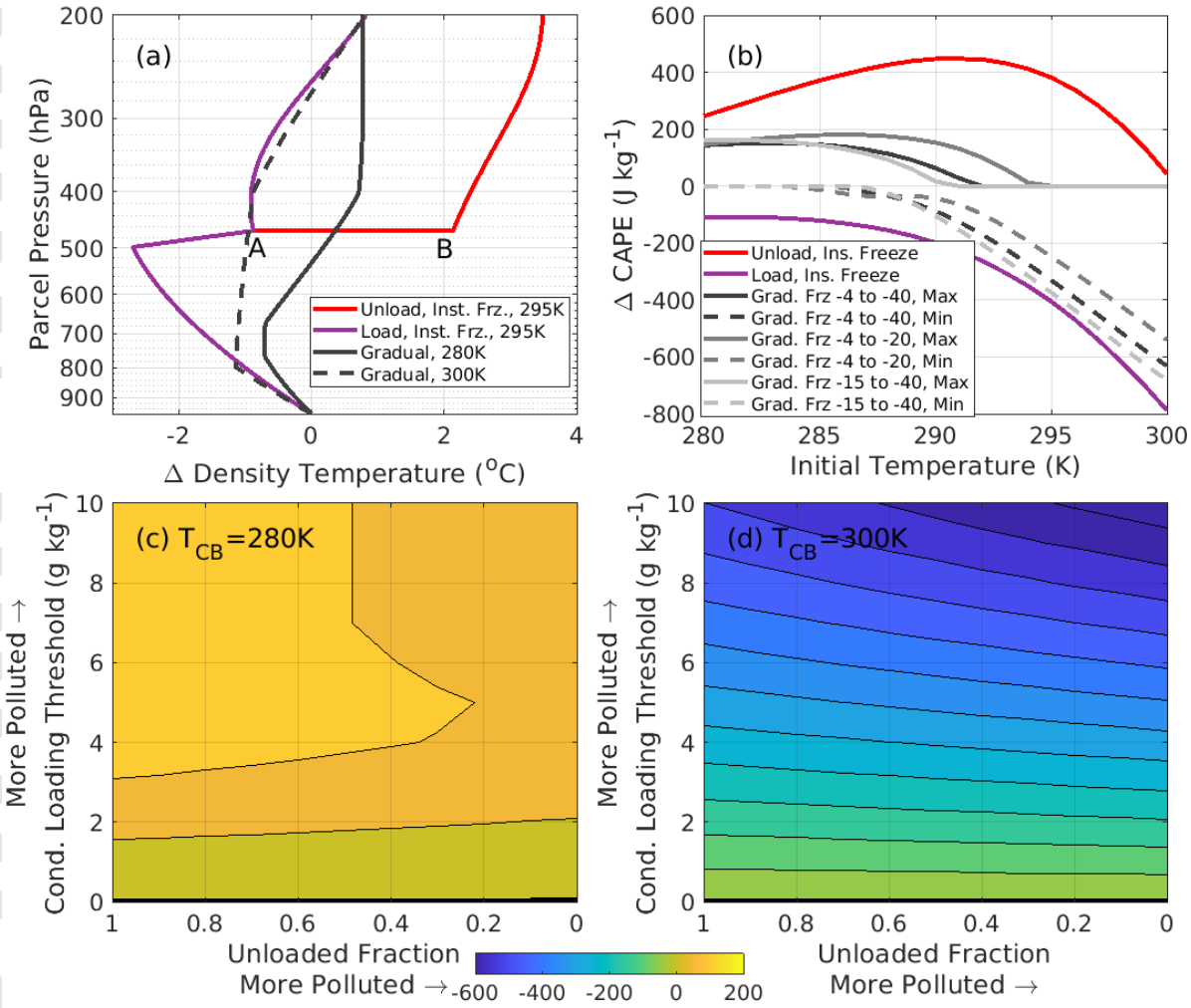

Fig. 1. (a) ΔT_ρ for various assumptions. The red and purple lines assume nearly instantaneous freezing, T_{CB}=295K, and condensate loading as described in the text. The dark gray solid

(dashed) line shows a sample profile with gradual freezing and unloading using T_{CB}=280K (300K). Labels A and B are referenced in the text. (b) ΔCAPE (J kg^{-1}) between polluted and ultra-clean parcels as a function of initial parcel temperature. The dark gray solid (dashed) line indicates the maximum (minimum) possible invigoration for the case of gradual unloading and gradual freezing between -4°C and -40°C. Medium (light) gray lines are the same except for gradual freezing between -4°C (-15°C) and -20°C (-40°C). (c-d) ΔCAPE (J kg^{-1}) between various polluted parcels and a parcel with no loading for (c) T_{CB}=280K and (d) T_{CB}=300K. Contours are drawn every 50 J kg^{-1} and all values are positive in (c) and negative in (d).

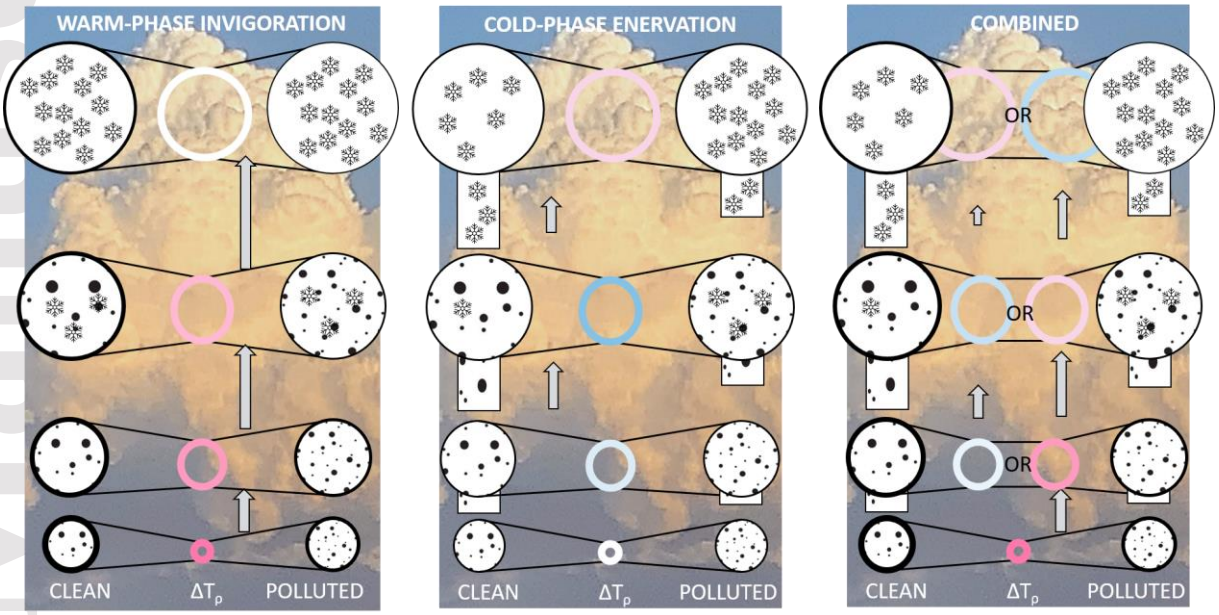

Fig. 2. A schematic representation of the major processes examined in this study for warm-based storms. Circles represent the parcel at multiple levels during its ascent. Circles increase in size with height as the parcels expand. Center circles are colored by the density temperature difference of the polluted and clean parcels, where warmer (colder) colors imply a positive (negative) difference. Arrows indicate differences in updraft speed between clean and polluted parcels and are drawn on the side corresponding to the parcel with stronger updrafts. The thickness of the parcel outline indicates the supersaturation and the length of the precipitation box below each parcel is proportional to the degree of unloading. The left panel shows the processes contributing to warm-phase invigoration, the central panel shows the processes contributing to cold-phase enervation, and the right panel shows two possible combination of effects.

3.2 Warm-phase invigoration

To quantify the potential invigoration from warm-phase processes, we arbitrarily consider an ultra-clean parcel as one which develops an equilibrium supersaturation of 20% during its ascent. Supersaturation of 10-15% has been simulated in tropical deep convection (Fan et al., 2018; Grabowski & Morrison, 2017) and supersaturation is presumably even larger in

midlatitude convection in which updrafts are typically stronger. Assumed profiles of supersaturation are shown in Figure 3a (see the supplemental information for the equation). In all calculations we assume no unloading of condensate and linear freezing between -4°C and -40°C.

Figure 3b shows that ΔCAPE increases as the equilibrium supersaturation decreases, that is, as the polluted parcels become more polluted. ΔCAPE due to aerosol loading is small in parcels with relatively cold T_{CB} and is much more substantial for parcels with a deep warm-phase, i.e. warmer T_{CB}. For a very polluted scenario of 0% supersaturation, the maximum ΔCAPE is slightly less than the maximum changes seen in Figure 1b (red line). ΔCAPE is about 25 J kg^{-1} (100 J kg^{-1}) for every 5% change in supersaturation for T_{CB}=280K (300K). Such a linear scaling of ΔT_ρ with supersaturation is also evident and was previously shown by Grabowski and Jarecka (2015).

Figures 3c and 3d illustrate that parcels with low supersaturation (i.e. more polluted parcels) are warmer than those with high supersaturation (i.e. cleaner parcels) due to the additional condensate formation and latent heat release (except near 200 hPa due to impacts of heat capacity). The maximum difference in condensate mass occurs around 700 hPa (Figure 2d). This indicates that at pressures lower than 700 hPa (higher heights), e.g., 600 hPa, a clean parcel is condensing mass faster than a polluted parcel. Such behavior is expected since both parcels must ultimately form nearly the same amount of condensate, regardless of supersaturation, by the time they reach 200 hPa as indicated in Figure 3d. Such behavior is also consistent with Grabowski and Jarecka (2015). The important point here is that the polluted parcel is not always condensing mass faster, but rather only condensing mass faster in the lowest levels. It is this which gives rise to an increase in parcel temperature that sustains its increased buoyancy throughout its rise. These results are illustrated schematically in the first panel of Figure 2.

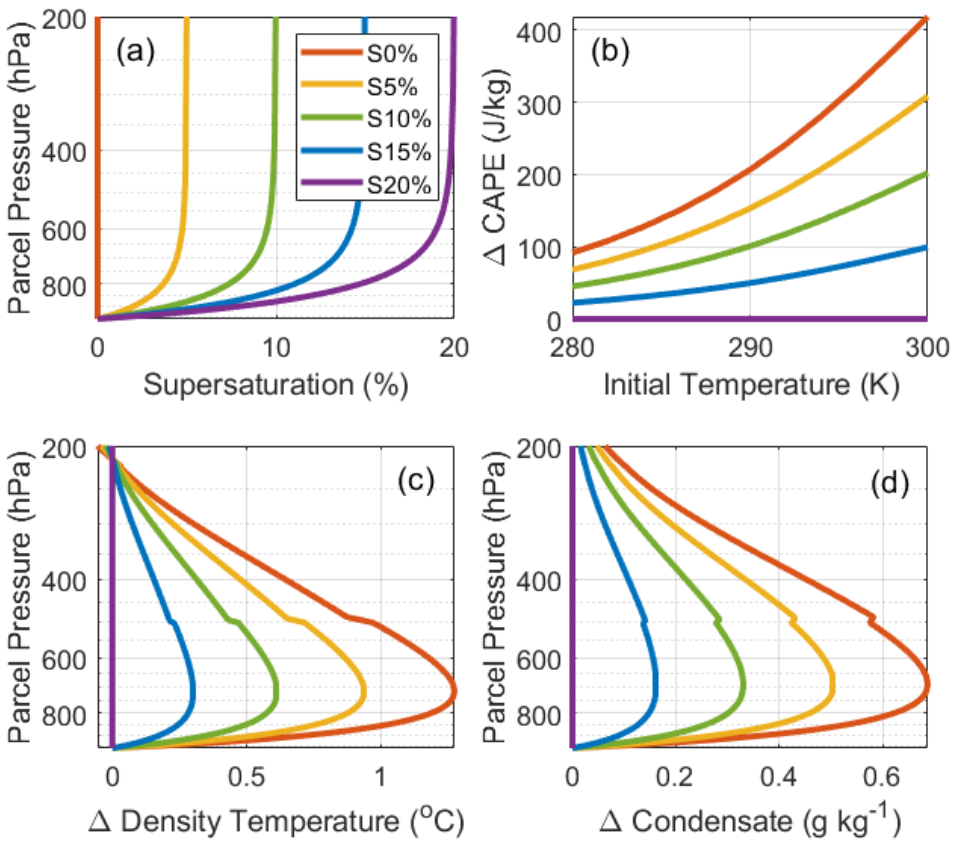

Fig. 3. (a) Specified profiles of supersaturation in the parcel calculations. Warmer colors indicate more polluted conditions. Differences between polluted parcels and an ultra-clean parcel with 20% supersaturation in (b) CAPE as a function of initial parcel temperature, (c) temperature as a function of parcel pressure, and (d) condensate as a function of parcel pressure. The parcels in (c-d) use T_{CB}=295 K.

3.3 Combined Effects

Based on the preceeding calculations, aerosol impacts to the warm-phase and cold-phase processes will often offset one another and minimize the total invigoration, particularly in warm-based storms. When considering the processes in both phases, ΔCAPE relative to an ultra-clean parcel for cold-based storms ranges from about 0 to 200 J kg^{-1} (Fig. 4a) whereas for warm-based storms it ranges from about -600 to 400 J kg^{-1} (Fig. 4b). The corresponding change in the maximum updraft speed depends on the updraft speed in the clean parcel. A maximum invigoration of 400 J kg^{-1} corresponds to increase in updraft speed of at most ~20 m s^{-1} in weak storms and ~5 m s^{-1} in strong storms (Eq. 4). These are likely overestimates given that CAPE is known to overpredict the maximum updraft speeds (Peters et al. 2020).

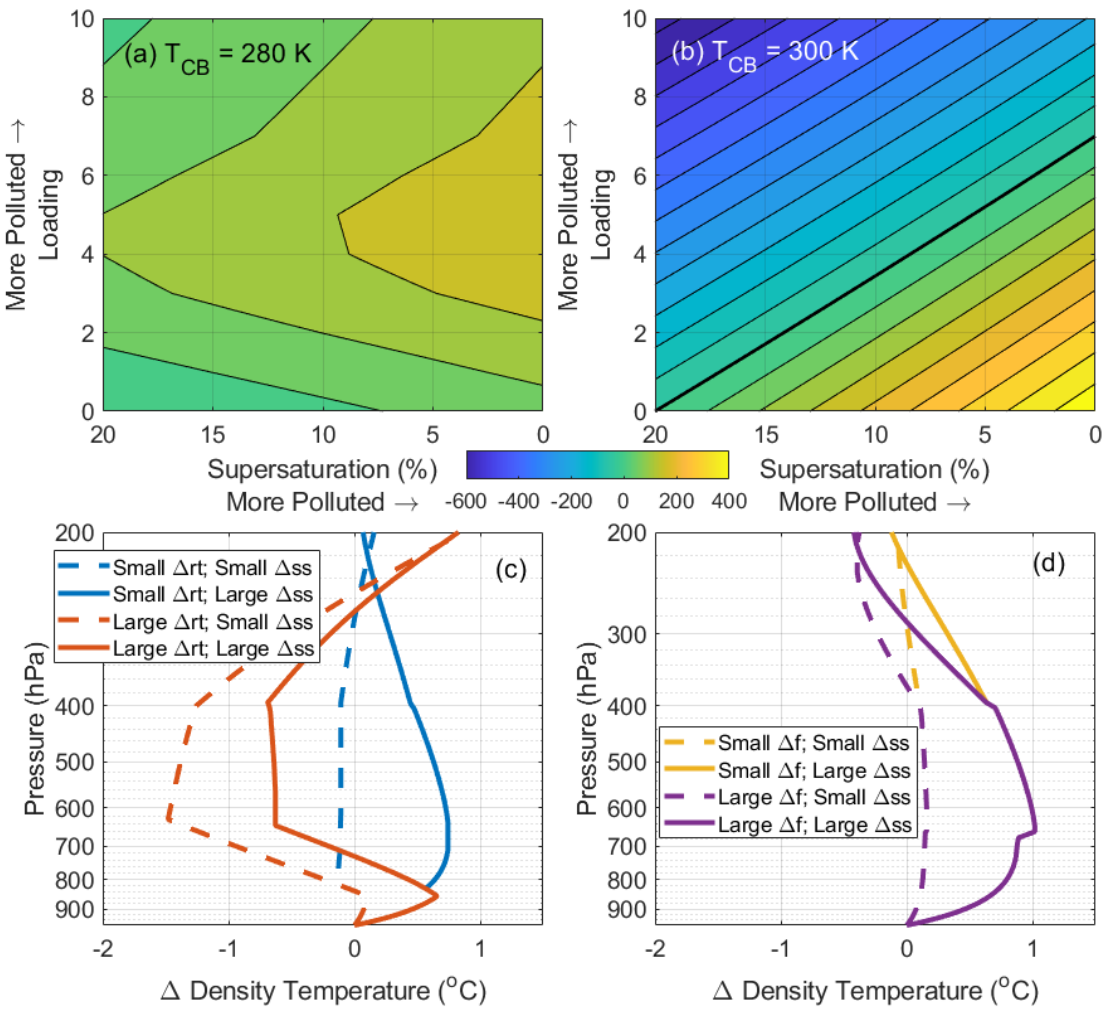

Fig. 4. (a-b) ΔCAPE (J kg^{-1}) relative to the cleanest parcel (highest supersaturation, no loading) as a function of supersaturation and loading with gradual freezing and gradual unloading as described in the text for (a) T_{CB}=280 K and (b) T_{CB}=300 K. The loading value indicates both the condensate loading threshold (g kg^{-1}) and the unloaded fraction (1-value/10) such that the two quantities vary simultaneously along the y-axis. Contours are drawn every 50 J kg^{-1} and the solid black line shows ΔCAPE = 0 J kg^{-1}. (c) ΔT_ρ corresponding to possible simultaneous changes in supersaturation (Δss, ss_{clean}=14%, ss_{poll}=12% or 0%) and condensate loading threshold (Δrt, rt_{clean}=2g kg^{-1}, rt_{poll}=3g kg^{-1} or 8g kg^{-1}). The unloaded fraction is held constant at 0.5. (d) Like (c) except for changes in the unloaded fraction (Δf, f_{clean}=0.8, f_{poll}=0.7 or 0.2) instead of loading threshold which is held constant at 7g kg^{-1}.

Example profiles of ΔT_ρ are shown in Figure 4c-d. Positive ΔT_ρ is evident at the lowest pressure levels due to initially greater condensation in the polluted parcel. The differences thereafter depend on whether changes in supersaturation, condensate loading threshold, or unloaded fraction dominate the response to an increase in CCN concentration. If changes in supersaturation dominate, the polluted parcel will remain more buoyant than the clean parcel throughout the ascent (Fig. 4c-d, solid blue and yellow lines). If the change in the condensate loading threshold dominates, the polluted parcel will be more buoyant than the clean parcel initially, less buoyant at midlevels and then more buoyant again at upper levels (Fig. 4c, red

lines). In this case, if we consider the relationship between buoyancy and vertical velocity, the polluted parcel may rise more quickly than the clean parcel initially, but rise more slowly thereafter. Finally, if the change to the fraction of unloaded precipitation dominates (Fig. 4d, purple lines), the polluted parcel may be less buoyant at the end of the ascent and so the polluted parcel rises fastest relative to the clean parcel at upper midlevels but below storm top. These examples demonstrate that invigoration may be a complex function of height depending on how the condensate loading and supersaturation are simultaneously impacted by aerosol concentration. The cases of dominant condensate loading threshold and dominant unloaded fraction are illustrated in the right panel of Figure 2 to highlight that there is some ambiguity in the combined effects of supersaturation and unloading on deep convective invigoration.

4 Conclusions

The theoretical calculations presented here suggest that aerosol-induced invigoration, that is, a CCN-induced (rather than ice nuclei-induced) increase in storm updraft speed, is theoretically possible, but is substantially smaller (and oftentimes even negative), than previous calculations suggested. The unrealistic assumptions regarding *instantaneous freezing and total condensate unloading* used by R08 greatly enhanced the estimated magnitude of invigoration. More realistic assumptions as those used here show that cold-phase invigoration is at best weakly positive and often contributes to storm weakening or enervation in environments with high aerosol loading, particularly in warm-based storms. That said, the nature of unloading and the rate of freezing in deep convection is unknown and as such we may have underestimated the cold-phase invigoration. Aerosol-induced invigoration is instead more likely driven by reduced supersaturation and enhanced condensation in the low levels of storms. As a result of storm invigoration in the warm-phase and possible storm enervation in the cold-phase, polluted storms may not be strongest relative to clean storms at storm top. Analysis of storm updraft speed changes as a function of height, particularly in the developing phase of storms, will help to elucidate these processes.

The magnitude of the aerosol-induced changes to CAPE are at most a few hundred J kg^{-1}. Changes in updraft speed are expected to be greatest in naturally weak storms, such as tropical convection. Finally, our calculations suggest that the magnitude of aerosol-induced invigoration will increase as the climate warms due to increased dominance of warm-phase invigoration. Current projections show up to 8K warming in the midlatitudes and up to 6K warming in the tropics (Fan et al., 2020). These projections correspond to an increase of up to ~90-120 J kg^{-1} in invigoration (Fig. 3b or inspection of Figs. 4a-b) and hence point to a continuing need to better understand this phenomenon.

Acknowledgments

S. C. van den Heever was supported by the Department of Energy Grant DE-SC0021160. Data figures and all code to reproduce the figures are publicly available at https://doi.org/10.25338/B8S044.

References

Abbott, T. H., & Cronin, T. W. (2021). Aerosol invigoration of atmospheric convection through increases in humidity. *Science, 371*(6524), 83-85. doi:10.1126/science.abc5181

Altaratz, O., Koren, I., Remer, L. A., & Hirsch, E. (2014). Review: Clouds invigoration by aerosols - coupling between microphysics and dynamics. *Atmospheric Research, 140-141*, 38-60. doi:10.1016/j.atmosres.2014.01.009

Andreae, M. O., Rosenfeld, D., Artaxo, P., Costa, A. A., Frank, G. P., Longo, K. M., & Silva-Dias, M. A. (2004). Smoking rain clouds over the Amazon. *Science, 303*(5662), 1337-1342. doi:10.1126/science.1092779

Chua, X. R., & Ming, Y. (2020). Convective Invigoration Traced to Warm- Rain Microphysics. *Geophysical Research Letters, 47*(23). doi:10.1029/2020gl089134

Emanuel, K. A. (1994). *Atmospheric Convection*: Oxford University Press.

Fan, J., Leung, L. R., Rosenfeld, D., Chen, Q., Li, Z., Zhang, J., & Yan, H. (2013). Microphysical effects determine macrophysical response for aerosol impacts on deep convective clouds. *Proc Natl Acad Sci U S A, 110*(48), E4581-4590. doi:10.1073/pnas.1316830110

Fan, J., Rosenfeld, D., Zhang, Y., Giangrande, S. E., Li, Z., Machado, L. A. T., et al. (2018). Substantial convection and precipitation enhancements by ultrafine aerosol particles. *Science, 359*(6374), 411-418. doi:10.1126/science.aan8461

Fan, J., Zhang, R., Li, G., & Tao, W.-K. (2007). Effects of aerosols and relative humidity on cumulus clouds. *Journal of Geophysical Research, 112*(D14). doi:10.1029/2006jd008136

Fan, X., Duan, Q., Shen, C., Wu, Y., & Xing, C. (2020). Global surface air temperatures in CMIP6: historical performance and future changes. *Environmental Research Letters, 15*(10), 104056. doi:10.1088/1748-9326/abb051

Früh, B., & Wirth, V. (2007). Convective Available Potential Energy (CAPE) in mixed phase cloud conditions. *Quarterly Journal of the Royal Meteorological Society, 133*(624), 561-569. doi:10.1002/qj.39

Grabowski, W. W. (2015). Untangling Microphysical Impacts on Deep Convection Applying a Novel Modeling Methodology. *Journal of the Atmospheric Sciences, 72*(6), 2446-2464. doi:10.1175/jas-d-14-0307.1

Grabowski, W. W. (2018). Can the Impact of Aerosols on Deep Convection be Isolated from Meteorological Effects in Atmospheric Observations? *Journal of the Atmospheric Sciences, 75*(10), 3347-3363. doi:10.1175/jas-d-18-0105.1

Grabowski, W. W., & Jarecka, D. (2015). Modeling Condensation in Shallow Nonprecipitating Convection. *Journal of the Atmospheric Sciences, 72*(12), 4661-4679. doi:10.1175/jas-d-15-0091.1

Grabowski, W. W., & Morrison, H. (2016). Untangling Microphysical Impacts on Deep Convection Applying a Novel Modeling Methodology. Part II: Double-Moment Microphysics. *Journal of the Atmospheric Sciences, 73*(9), 3749-3770. doi:10.1175/jas-d-15-0367.1

Grabowski, W. W., & Morrison, H. (2017). Modeling Condensation in Deep Convection. *Journal of the Atmospheric Sciences, 74*(7), 2247-2267. doi:10.1175/jas-d-16-0255.1

Grabowski, W. W., & Morrison, H. (2020). Do Ultrafine Cloud Condensation Nuclei Invigorate Deep Convection? *Journal of the Atmospheric Sciences, 77*(7), 2567-2583. doi:10.1175/jas-d-20-0012.1

Grant, L. D., & van den Heever, S. C. (2015). Cold Pool and Precipitation Responses to Aerosol Loading: Modulation by Dry Layers. *Journal of the Atmospheric Sciences, 72*(4), 1398-1408. doi:10.1175/jas-d-14-0260.1

Hu, J., Rosenfeld, D., Ryzhkov, A., Zrnic, D., Williams, E., Zhang, P., et al. (2019). Polarimetric Radar Convective Cell Tracking Reveals Large Sensitivity of Cloud Precipitation and Electrification Properties to CCN. *Journal of Geophysical Research: Atmospheres, 124*(22), 12194-12205. doi:10.1029/2019jd030857

Hu, Y., Rodier, S., Xu, K.-m., Sun, W., Huang, J., Lin, B., et al. (2010). Occurrence, liquid water content, and fraction of supercooled water clouds from combined CALIOP/IIR/MODIS measurements. *Journal of Geophysical Research, 115*. doi:10.1029/2009jd012384

Khain, A., Rosenfeld, D., & Pokrovsky, A. (2005). Aerosol impact on the dynamics and microphysics of deep convective clouds. *Quarterly Journal of the Royal Meteorological Society, 131*(611), 2639-2663. doi:10.1256/qj.04.62

Kogan, Y. L., & Martin, W. J. (1994). Parameterization of Bulk Condensation in Numerical Cloud Models. *Journal of the Atmospheric Sciences, 51*(12), 1728-1739. doi:10.1175/1520-0469(1994)051<1728:POBCIN>2.0.CO;2

Koren, I., Dagan, G., & Altaratz, O. (2014). From aerosol-limited to invigoration of warm convective clouds. *Science, 344*(6188), 1143-1146. doi:10.1126/science.1252595

Koren, I., Kaufman, Y. J., Rosenfeld, D., Remer, L. A., & Rudich, Y. (2005). Aerosol invigoration and restructuring of Atlantic convective clouds. *Geophysical Research Letters, 32*(14), n/a-n/a. doi:10.1029/2005gl023187

Lebo, Z. (2018). A Numerical Investigation of the Potential Effects of Aerosol-Induced Warming and Updraft Width and Slope on Updraft Intensity in Deep Convective Clouds. *Journal of the Atmospheric Sciences, 75*(2), 535-554. doi:10.1175/jas-d-16-0368.1

Lebo, Z. J., & Seinfeld, J. H. (2011). Theoretical basis for convective invigoration due to increased aerosol concentration. *Atmospheric Chemistry and Physics, 11*(11), 5407-5429. doi:10.5194/acp-11-5407-2011

Lerach, D. G., Gaudet, B. J., & Cotton, W. R. (2008). Idealized simulations of aerosol influences on tornadogenesis. *Geophysical Research Letters, 35*(23). doi:10.1029/2008gl035617

Li, Z., Niu, F., Fan, J., Liu, Y., Rosenfeld, D., & Ding, Y. (2011). Long-term impacts of aerosols on the vertical development of clouds and precipitation. *Nature Geoscience, 4*(12), 888-894. doi:10.1038/ngeo1313

Marinescu, P. J., van den Heever, S. C., Heikenfeld, M., Barrett, A. I., Barthlott, C., Hoose, C., et al. (2021). Impacts of Varying Concentrations of Cloud Condensation Nuclei on Deep Convective Cloud Updrafts—A Multimodel Assessment. *Journal of the Atmospheric Sciences, 78*(4), 1147-1172. doi:10.1175/jas-d-20-0200.1

Morrison, H. (2012). On the robustness of aerosol effects on an idealized supercell storm simulated with a cloud system-resolving model. *Atmospheric Chemistry and Physics, 12*(16), 7689-7705. doi:10.5194/acp-12-7689-2012

Peters, J. M., Morrison, H., Nowotarski, C. J., Mulholland, J. P., & Thompson, R. L. (2020). A formula for the maximum vertical velocity in supercell updrafts. *Journal of the Atmospheric Sciences, 77*, 3747-3757. doi:10.1175/JAS-D-20-0103.1

Pinsky, M., Mazin, I. P., Korolev, A., & Khain, A. (2013). Supersaturation and Diffusional Droplet Growth in Liquid Clouds. *Journal of the Atmospheric Sciences, 70*(9), 2778-2793. doi:10.1175/jas-d-12-077.1

Rosenfeld, D., Lohmann, U., Raga, G. B., O'Dowd, C. D., Kulmala, M., Fuzzi, S., et al. (2008). Flood or drought: how do aerosols affect precipitation? *Science, 321*(5894), 1309-1313. doi:10.1126/science.1160606

Saleeby, S. M., Herbener, S. R., van den Heever, S. C., & L'Ecuyer, T. (2015). Impacts of Cloud Droplet–Nucleating Aerosols on Shallow Tropical Convection. *Journal of the Atmospheric Sciences, 72*(4), 1369-1385. doi:10.1175/jas-d-14-0153.1

Seiki, T., & Nakajima, T. (2014). Aerosol Effects of the Condensation Process on a Convective Cloud Simulation. *Journal of the Atmospheric Sciences, 71*(2), 833-853. doi:10.1175/jas-d-12-0195.1

Sheffield, A. M., Saleeby, S. M., & van den Heever, S. C. (2015). Aerosol-induced mechanisms for cumulus congestus growth. *Journal of Geophysical Research: Atmospheres, 120*(17), 8941-8952. doi:10.1002/2015jd023743

Stolz, D. C., Rutledge, S. a., & Pierce, J. R. (2015). Simultaneous influences of thermodynamics and aerosols on deep convection and lightning in the tropics. *Journal of Geophysical Research: Atmospheres, 120*, 6207-6231. doi:10.1002/2014JD023033.Received

Storer, R. L., & van den Heever, S. C. (2013). Microphysical Processes Evident in Aerosol Forcing of Tropical Deep Convective Clouds. *Journal of the Atmospheric Sciences, 70*(2), 430-446. doi:10.1175/jas-d-12-076.1

Storer, R. L., van den Heever, S. C., & L'Ecuyer, T. S. (2014). Observations of aerosol-induced convective invigoration in the tropical east Atlantic. *Journal of Geophysical Research: Atmospheres, 119*(7), 3963-3975. doi:10.1002/2013jd020272

Storer, R. L., van den Heever, S. C., & Stephens, G. L. (2010). Modeling Aerosol Impacts on Convective Storms in Different Environments. *Journal of the Atmospheric Sciences, 67*(12), 3904-3915. doi:10.1175/2010jas3363.1

Tao, W.-K., Chen, J.-P., Li, Z., Wang, C., & Zhang, C. (2012). Impact of aerosols on convective clouds and precipitation. *Reviews of Geophysics, 50*(2). doi:10.1029/2011rg000369

Thornton, J. A., Virts, K. S., Holzworth, R. H., & Mitchell, T. P. (2017). Lightning enhancement over major oceanic shipping lanes. *Geophysical Research Letters, 44*(17), 9102-9111. doi:10.1002/2017gl074982

van den Heever, S. C., Carrió, G. G., Cotton, W. R., DeMott, P. J., & Prenni, A. J. (2006). Impacts of Nucleating Aerosol on Florida Storms. Part I: Mesoscale Simulations. *Journal of the Atmospheric Sciences, 63*(7), 1752-1775. doi:10.1175/JAS3713.1

van den Heever, S. C., Stephens, G. L., & Wood, N. B. (2011). Aerosol Indirect Effects on Tropical Convection Characteristics under Conditions of Radiative–Convective Equilibrium. *Journal of the Atmospheric Sciences, 68*(4), 699-718. doi:10.1175/2010jas3603.1

Xu, K.-M., & Emanuel, K. A. (1989). Is the Tropical Atmosphere Conditionally Unstable? *Monthly Weather Review, 117*(7), 1471-1479. doi:10.1175/1520-0493(1989)117<1471:ittacu>2.0.co;2